Journal of Geochemical Exploration 158 (2015) 10–21

Contents lists available at ScienceDirect

Journal of Geochemical Exploration

journal homepage: www.elsevier.com/locate/jgeoexp

Multi-Gaussian kriging: a practice to enhance delineation of mineralized zones by Concentration–Volume fractal model in Dardevey iron ore deposit, SE Iran

Peyman Afzal [a,b,*], Nasser Madani [c,d], Shahab Shahbeik [a], Amir Bijan Yasrebi [b]

[a] Department of Mining Engineering, South Tehran Branch, Islamic Azad University, Tehran, Iran
[b] Camborne School of Mines, University of Exeter, Penryn, UK
[c] Department of Mining Engineering, University of Chile, Santiago, Chile
[d] Advanced Mining Technology Center, University of Chile, Santiago, Chile

ARTICLE INFO

Article history:
Received 19 December 2014
Revised 13 June 2015
Accepted 21 June 2015
Available online 28 June 2015

Keywords:
Ordinary multi-Gaussian kriging (oMK)
Simple multi-Gaussian kriging (sMK)
Variance
Concentration–Volume (C–V) fractal modeling
Dardevey

ABSTRACT

The purpose of this study is to identify the effect of ordinary and simple multi-Gaussian kriging (oMK, sMK) estimation methods for the delineation of iron mineralized zones based on subsurface data using Concentration–Volume (C–V) fractal modeling in the Dardevey iron ore deposit, NE Iran. Spatial data analyses (variograms and anisotropic ellipsoid) were initially calculated for the Fe distribution. The C–V log–log plots based on the estimation methods represent the various mineralized zones via threshold values. Additionally, variance in the both methods was compared. The comparison and interpretation of the mineralized zones based on the C–V fractal modeling show that the methods are similar, but the enriched and highly zones resulted by the oMK have variances lower than the sMK method. Furthermore, the weakly and moderately mineralized zones have lower variances based on the sMK method. According to the comparison and variance, optimum threshold values for enriched, highly, moderately and weakly iron mineralized zones are 56%, 51%, 41% and 35%, respectively.

1. Introduction

Fractal/multifractal modeling established by Mandelbrot (1983) has been widely applied in different geoscience branches especially in the spatial modeling of different mineralized zones and geochemical anomalies (e.g., Afzal et al., 2011, 2012; Agterberg et al., 1993; Carranza, 2008; Cheng et al., 1994; Cheng, 1999, 2007; Heidari et al., 2013; Li et al., 2002, 2003, 2004; Lima et al., 2003; Ma et al., 2014; Zuo et al., 2009, 2012, 2013; Zuo and Wang, 2015). The Concentration–Volume (C–V) fractal model proposed by Afzal et al. (2011) can be utilized to distinguish various mineralized zones with respect to the threshold values (breakpoints). As a result, the C–V fractal model is considered as a proper method to describe spatial distributions of different attributes (ore elements in this scenario) within the various orebodies (Agterberg, 2012; Cheng and Agterberg, 2009; Sadeghi et al., 2012; Daneshvar et al., 2012; Yasrebi et al., 2014).

Geostatistical tools have been considered as a powerful technique for the purpose of uncertainty quantification where the mineral grade is greater than the specific thresholds as an application to delineate geochemical populations, mining, petroleum engineering and soil contamination (Benndorf and Dimitrakopoulos, 2013; Chilès and Delfiner, 2012; Emery, 2007; Mao and Journel, 1999; Pyrcz and Deutsch, 2014; Reis et al., 2003; Stegman, 2001; Subbey et al., 2004).

Selection of a proper estimation method is significantly critical for fractal/multifractal approach especially for the C–V modeling which behaves towards detection of threshold values for enhanced separation of geological populations. Linear geostatistics such as conventional approaches of kriging is unsuitable as a consequence of smoothing property which suffers from order relation problems and requires the variogram to be calculated in terms of cut-offs therefore; the results are unrealistic from the practical point of view (over and under estimation: Chilès and Delfiner, 2012; Cressie and Johannesson, 2001; Deutsch and Journel, 1998; Costa, 2003). Other alternatives covering non-linear spatial interpolation as indicators can be named as “disjunctive” and “multi-Gaussian kriging” which have been widely accepted due to no order relation problem and smoothing effect. Two forms of multi-Gaussian kriging called simple and ordinary were proposed for recoverable resource assessments and mapping the probabilities. The simple multi-Gaussian kriging assumes that the mean value is perfectly known through the region and then restricts its usage (Emery, 2008; Guibal and Remacre, 1984; Mare'chal, 1984; Schofield, 1988). Conversely, ordinary multi-Gaussian kriging on the basis of unknown mean regarding mild assumption for driving an unbiased estimator was first coined by Emery (2006a,b). This model relies on the “pseudo” conditional distribution instead of “true” distribution which cannot assess the local uncertainty. In this respect, they don't have the same

* Corresponding author.
E-mail address: P_Afzal@azad.ac.ir (P. Afzal).

http://dx.doi.org/10.1016/j.gexplo.2015.06.011
0375-6742/

distribution as the true one which is a practical issue in the fractal modeling. To overcome this impediment, Emery (2008) proposed a new approach to substitute the unknown mean for random variable constant through the region and advantageously, the true conditional distribution could be met. This method is highly recommended in the case of some domains including trend in the variability of attribute under study whereas universal kriging is problematic in variogram analysis (Armstrong, 1984; Cressie, 1987; Matheron, 1971). However, in practice, the characterization of the attribute distribution influences results obtained by kriging (Deutsch and Rossi, 2014).

The main aim of this paper is to compare the accuracy and variance of different mineralized zones which were derived by the C–V fractal model based on ordinary multi-Gaussian (oMK) and simple kriging (Msk) interpolation methods in the Dardevey iron ore deposit, NE Iran.

2. Methodology

2.1. Multi-Gaussian kriging

Multi-Gaussian models are applicable in the sense of non-linear estimation and geostatistical simulation (Chilès and Delfiner, 2012; Verly, 1984). The related assumption is with respect to normalization of underlying attribute to Gaussian random field regarding the mean 0 and unit variance. Simple kriging type of this approach implies that any estimation of a random field is still Gaussian with the mean and variance identical to the simple kriging spatial prediction. The related formula is as follows (David, 1970; Rivoirard, 1994; Verly, 1983):

$$[f(Y_x)]^{sMK} = \int f\left(y_x^{sk} + \partial_x^{sk} u\right) g(u) du \quad (1)$$

where:

$f(T_x)$ the function of standard Gaussian variable
$[f(Y_x)]^{sMK}$ simple multi-Gaussian kriging
y_x^{sk} simple kriging estimation
∂_x^{sk} simple kriging variance
$g(u)$ The standard Gaussian pdf.

With respect to the assumption of constant mean, simple multi-Gaussian kriging is restricted and is not satisfactory. The crucial drawback is impractical evaluation in the case of inaccurate particularization

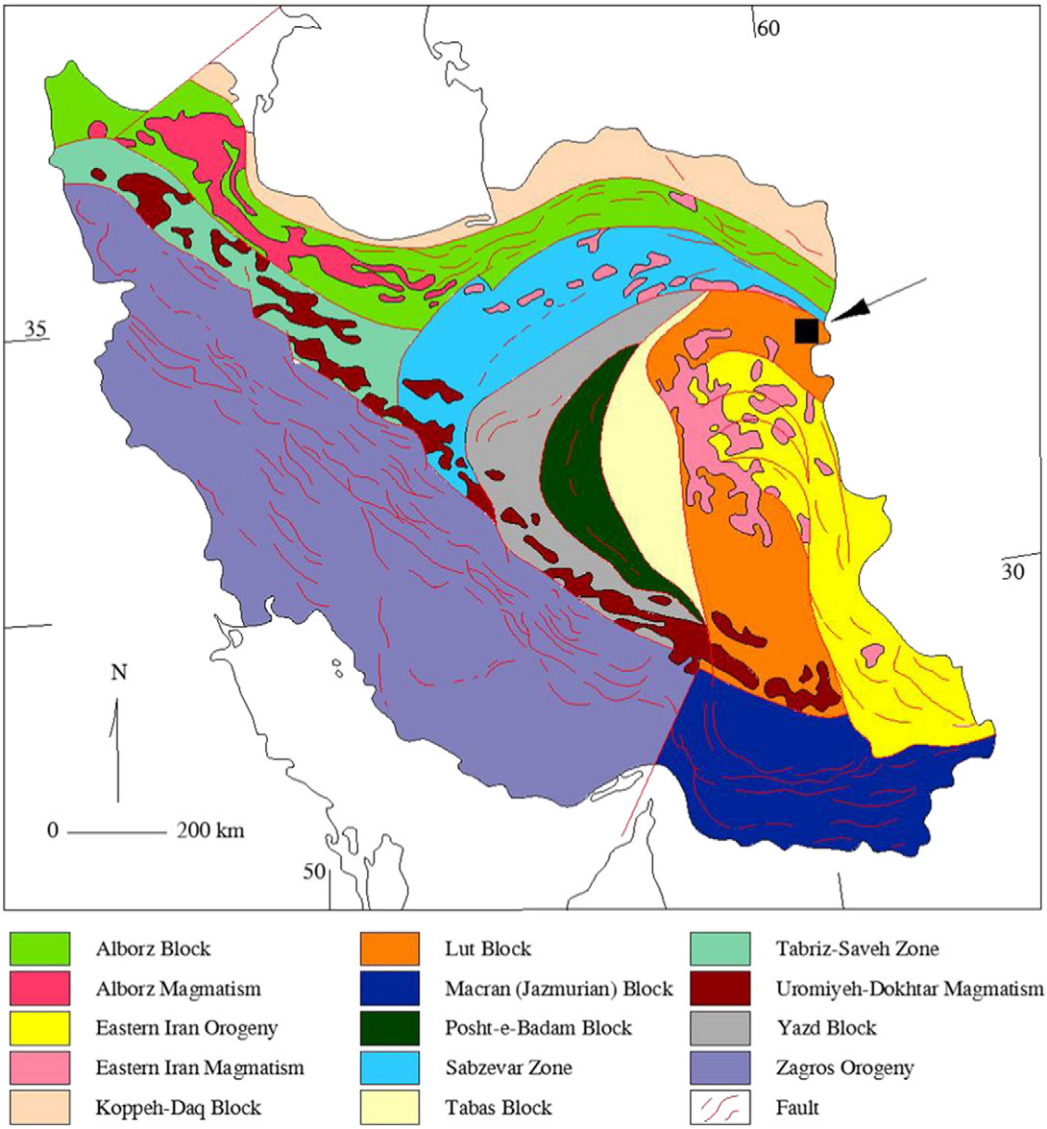

Fig. 1. Location of studied area in structural map of Iran (Black Square; Stocklin 1977).

of the mean. A substitution, which is more common in the practical consideration, is ordinary multi-Gaussian kriging for the sake of overcoming this condition. Emery (2006a,b,c) proposed the assumption of ordinary multi-Gaussian kriging to make the estimator more wide spread-used and robust to the non-stationary variability in the domain by replacing the unknown mean by random variable constant over the space. Some researchers recommended implementing the ordinary kriging but maintaining the simple kriging variance which is

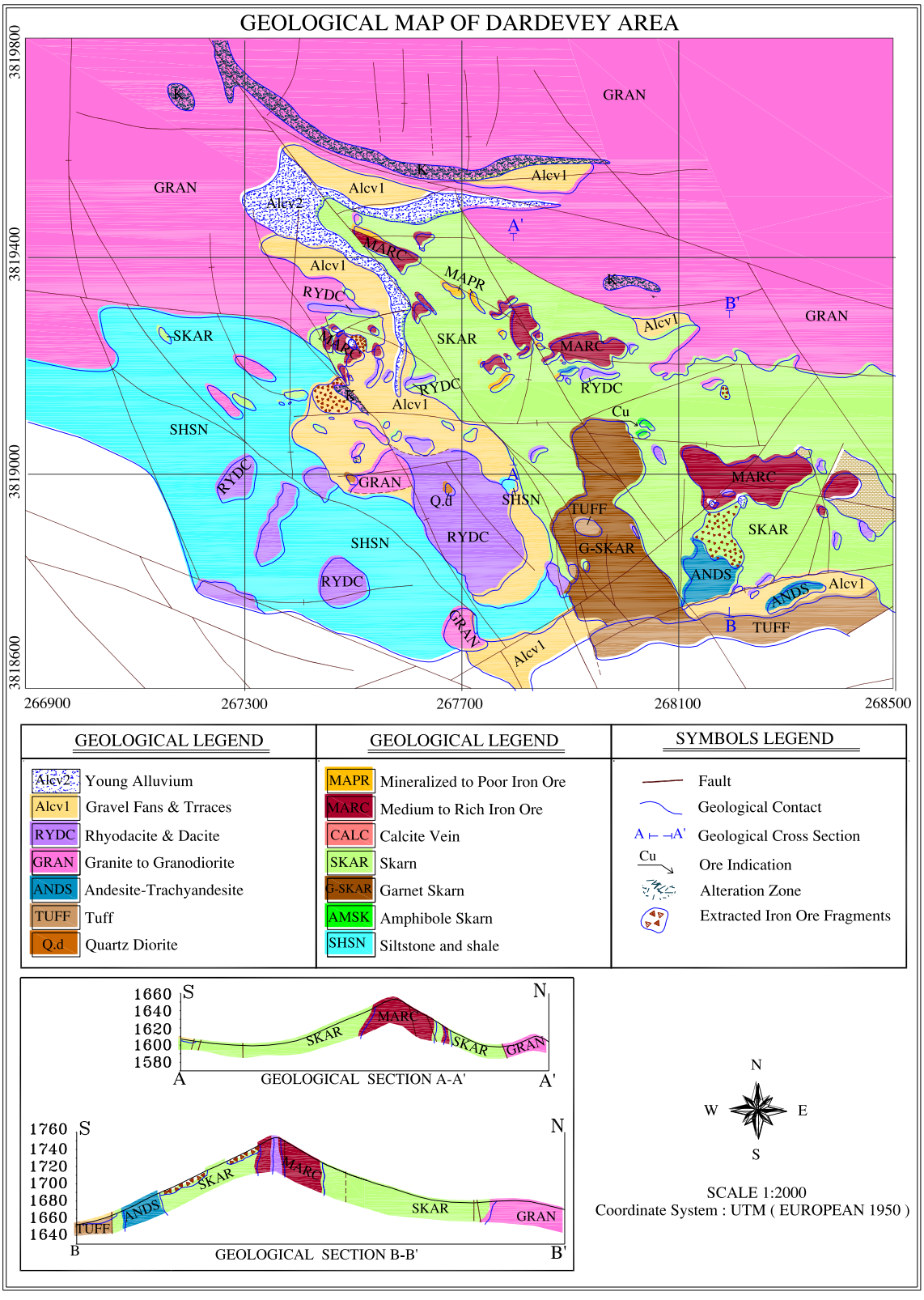

Fig. 2. Geological and structural map of the studied area (Hasanipack et al., 2009).

comprehensively imprecise (Goovaerts, 1997; Journel, 1980). Emery (2006c) was warned against this point. Hence, the ordinary multi-Gaussian kriging can be defined as the follow:

$$[f(Y_x)]^{oMK} = \int f(y) g_x^{ok}(y|data)dy \quad (2)$$

where

$g_x^{ok}(y|data)$ is the Gaussian pdf with mean equal to y_x^{ok} and variance $(\partial_x^{ok})^2 + 2\mu_x$

$[f(Y_x)]^{oMK}$ Ordinary multi-Gaussian kriging.

In order to implement the multi-Gaussian kriging, it is suggested to follow the consecutive procedures:

- Normal score transformation of the raw data
- Variogram analysis over the Gaussian variables
- Estimation of the Gaussian variables (simple or ordinary) and cross-validation
- Back transformation to the original database

2.2. C–V fractal model

The C–V fractal model proposed by Afzal et al. (2011) is used to delineate the different mineralized zones in order to characterize the

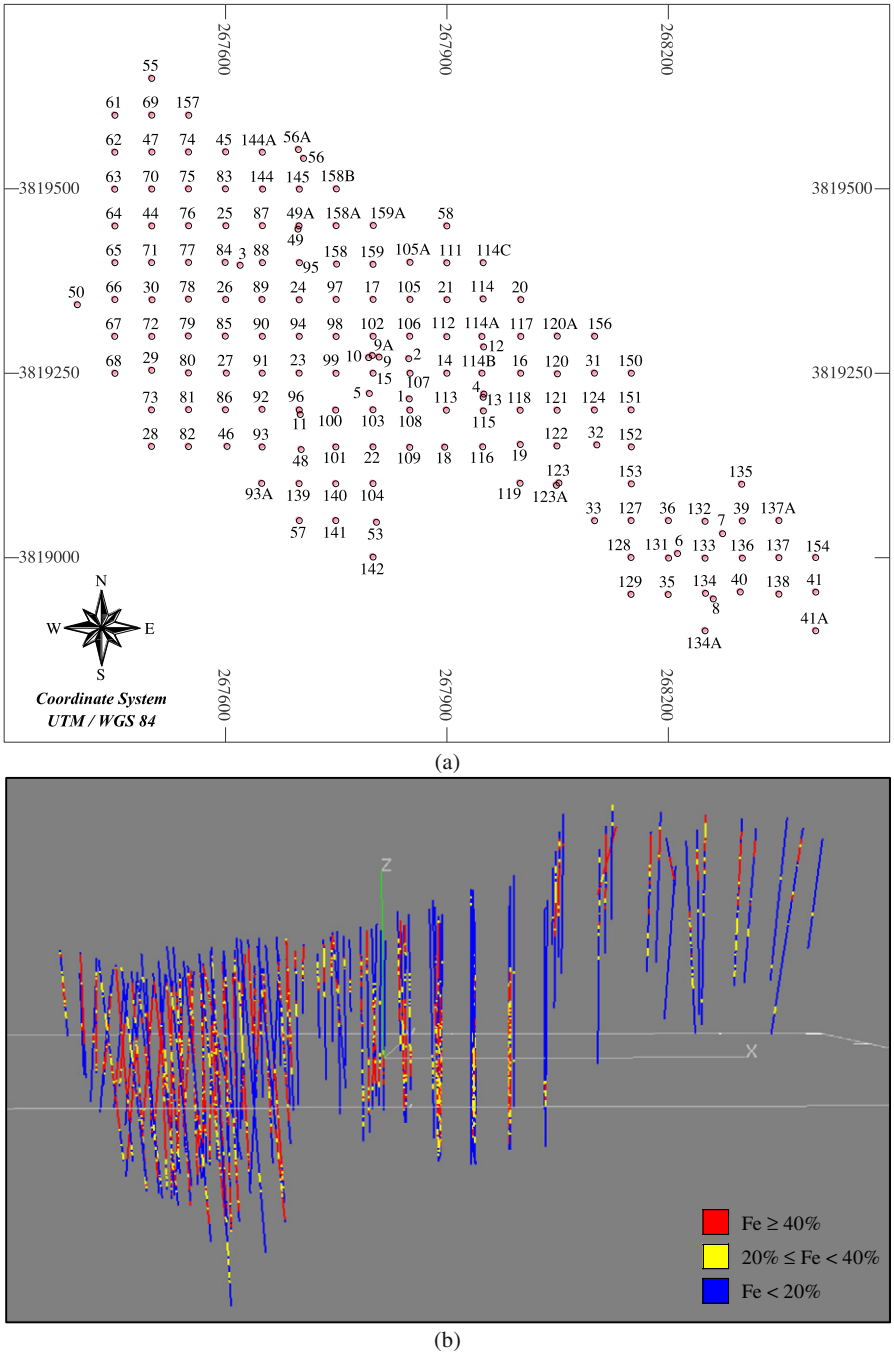

Fig. 3. 2D (a), 3D drillcore location map (b) and sampling location for elevation 1574.11 m (c: Shahbeik et al. 2014).

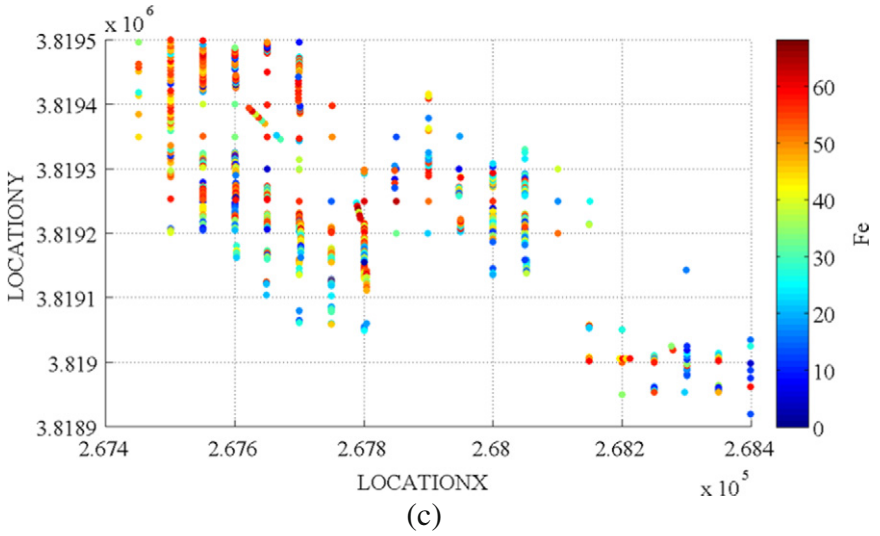

Fig. 3 (*continued*).

distribution of major, minor or paragenesis elemental concentrations in relation to different types of deposits such as Cu porphyry, Pb–Zn with carbonate host rocks, orogenic and epithermal gold, coal seams and iron ores (e.g., Afzal et al., 2013, 2014; Delavar et al., 2012; Sadeghi et al., 2012; Yasrebi et al., 2013). This model is expressed in the following form:

$$V(\rho < \upsilon) \propto \rho^{-a1}; \quad V(\rho \geq \upsilon) \propto \rho^{-a2} \tag{3}$$

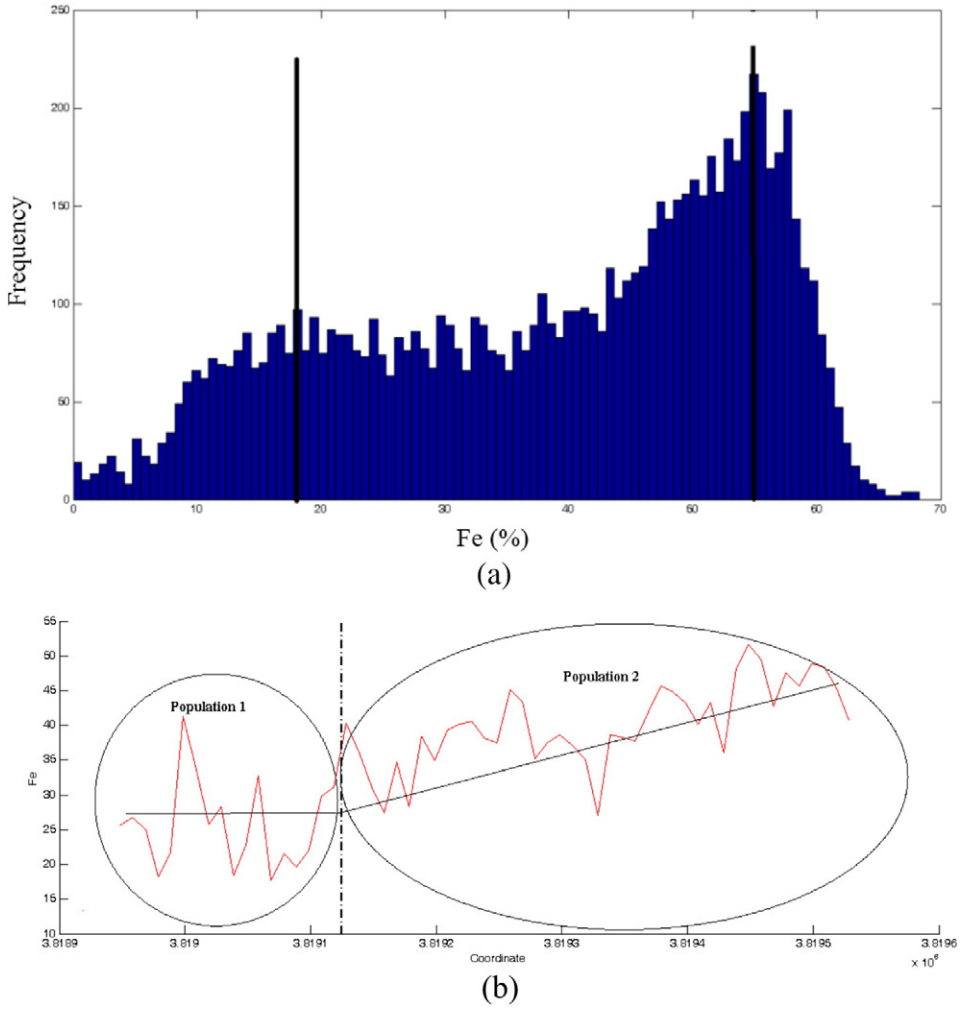

Fig. 4. Fe (%) histogram (a) and Fe trend analysis for the north direction (b).

where, $V(\rho < \upsilon)$ and $V(\rho \geq \upsilon)$ indicate volumes (V) with concentration values (ρ) that are, respectively, smaller and greater than contour values (υ), which define those volumes, and a1 and a2 are exponents. In the log–log plots, elemental concentration values versus volume, certain concentration contours (υ) represent threshold values (breakpoints) which distinguish the mineralized zones in the different types of the ore deposit according to distinct geochemical processes. Threshold values recognized by the means of the C–V fractal model are likely to address the boundaries between different ore zones (Wang et al., 2013; Rahmati et al., 2015; Soltani et al., 2014).

To calculate $V(\rho < \upsilon)$ and $V(\rho \geq \upsilon)$ enclosed by a concentration contour in a 3D model, e.g., the original drillcore data of the ore element and corresponding concentrations were interpolated using the oMK and sMK estimation methods.

3. Geological setting of Dardevey deposit

The world-class Sangan iron skarn deposit is located in the Khaf–Kashmar–Bardaskan Volcano-Plutonic Metallogenic Belt (NE Iran) with a proven reserve of > 1000 Mt iron ore and 53% Fe. Skarn mineralization happens at the contact of the 39.1 ± 0.6 Ma to 38.3 ± 0.5 Ma Middle Eocene syenite to syenogranite porphyry pluton with Cretaceous carbonate rocks (Malekzadeh Shafaroudi et al., 2013; Golmohammadi et al., 2015). The Sangan complex consists of several ore bodies such as Dardevey, Baghak, A, A′, B, C and C North. The Dardevey deposit is situated about 18 km NE of Sangan, as shown in Fig. 1. This area is located in the Lut structural zone, which is one of the subdivisions of the Iranian central structural zone at north Darouneh fault, as depicted in Fig. 1. Dardevey iron ore includes a Fe skarn system and the metallic minerals in Dardevey deposit are magnetite, hematite, Goethite, pyrite, martite (Hasanipack et al., 2009).

The Dardevey deposit is located in the southern margin of the Upper Eocene SarNowsar granite (biotite-amphibole granite) and occurs in an east–west trending sequence of Upper Mesozoic sedimentary rocks. The Magnetite skarn is formed in the black limestone and dolomite (Jurassic–Lower Cretaceous). They are considered massive and in some localities, they are around t 200 m thick. Mineral paragenesis is magnetite ± hematite ± pyrite and some chalcopyrite ± garnet (andradite) ± actinolite ± chlorite ± phlogopite calcite ± dolomite. The Dardevey deposit is Mg-skarn and the Mg content of agnetite is around 1.22–1.26%. At least four stages of skarn formation and ore deposition have been recognized within the area (stages I, II, III and IV a, b). Based on satellite images and field observation, the Dardevey deposit was displaced by a strike slip fault more than one Km from the Baghak deposit (Ghavi and Karimpour, 2010).

Exploration drill cores and surface magnetic surveys in the study area confirmed this motion and dips of the mineralized zone which are inclined towards the South (80°–85°). The recognition of a fault system and structural features are important because these may materially affect the assessment and exploration of other segments of the hidden ore body. In addition, the main structural features are two fault systems trending the NW–SE and E–W, as depicted in (Fig. 2: Ghavi and Karimpour, 2010).

4. Descriptive analysis

The dataset consists of 8456 samples with intervals of 2 m for each originating from 156 exploration drillholes (Fig. 3) and the Fe

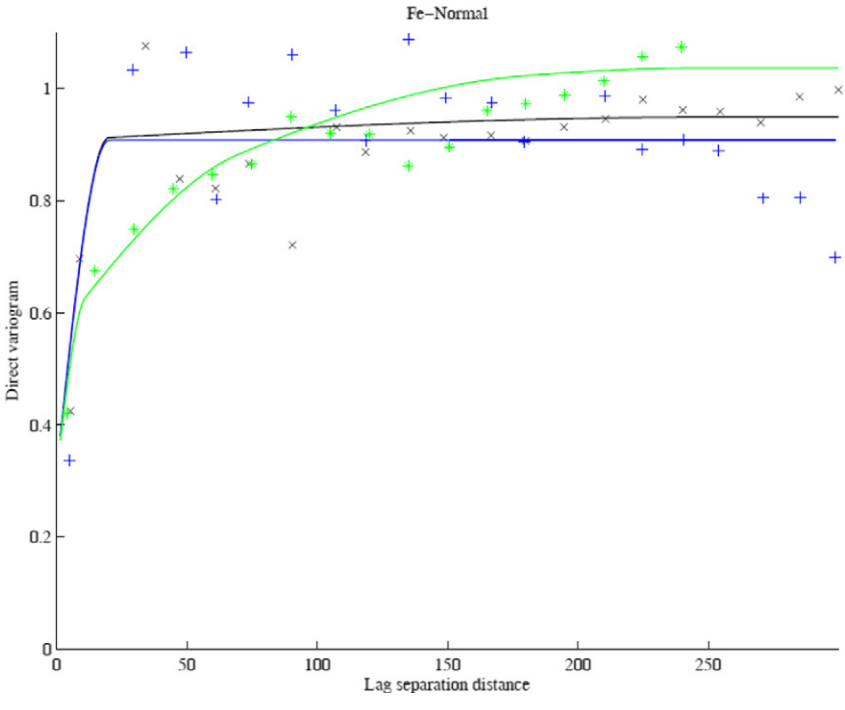

Green: Azimuth: -45, Dip: 0, (Horizontal)

Black: Azimuth: 45, Dip: 0,(Horizontal)

Blue: Azimuth: 0, Dip: 90 (Vertical)

Fig. 5. Semi-Variogram analysis; experimental along with theoretical model.

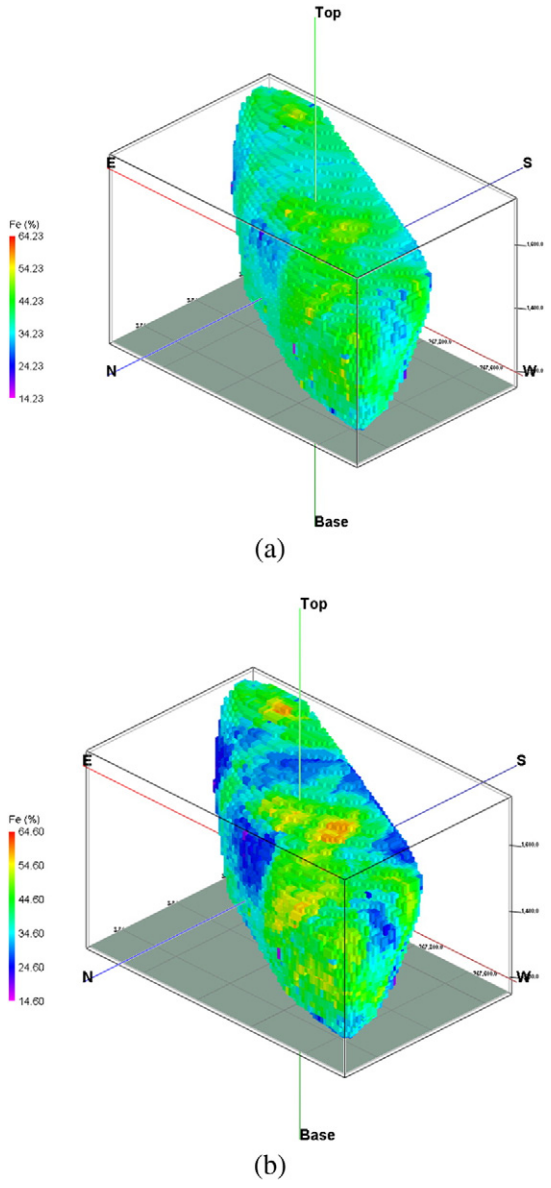

Fig. 6. Fe block models based on sMK (a) and oMK (b).

Table 1
Cross-validation parameters.

	MSE	MAE	ME	MEDE	STDE
Ordinary	88.65	6.94	0.12	1.70	9.41
Simple	88.73	6.99	0.12	1.76	9.41

MSE: mean square error; MAE: mean absolute error; ME: mean error; MEDE: median error; STDE: standard deviation of error.

grade has been assayed over the samples. The empirical histogram produced by cell de-clustering method to preserve the representativeness of the distribution to show that two populations are probable (Goovaerts, 1997: Fig. 3). Bimodality of the histogram analysis is perfectly undimmed in the distribution. One may be interested to separate more populations by fractal methodology. To implement any geostatistical methodology, it is of interest to check the variability of the underlying attribute over the region in which the trend exists. This issue is helpful for the good sense of decision on applying the simple or ordinary kriging, with the assumption of stationary. The most common practical technique is to consider the variability of the attribute versus the principal coordinates. As can be seen from the Fig. 4, the trend analysis in the north direction presents two distinct regions. This is consistent with the two populations obtained by the descriptive analysis of the histogram (Fig. 4). In the first population, the variability of the Fe fluctuates around a constant mean pretending the stationary while in the second population, the Fe grade depends on the location and increases with a mild slope, in which it presents non-stationary assumption. With respect to this trend analysis, one encourages applying simple and/or ordinary kriging (the trend in this random direction is presented to save the space). The goodness of the methodologies of estimation is discussed hereafter.

5. Spatial data analysis

Gaussian anamorphosis is incorporated for transferring declustered Fe variables to a standard Gaussian random field as the initial phase of multi-Gaussian kriging includes mean and variance close to zero and one, respectively. In order to analyze the spatial variability, the semi-variogram is calculated along the prespecified main directions of anisotropy as can be seen in Fig. 5 (Horizontal: −45°, with the practical range of 250 m and 45 orthogonal to that direction with the practical range of 20 m and a vertical direction with the 20 m range). The five nested structures

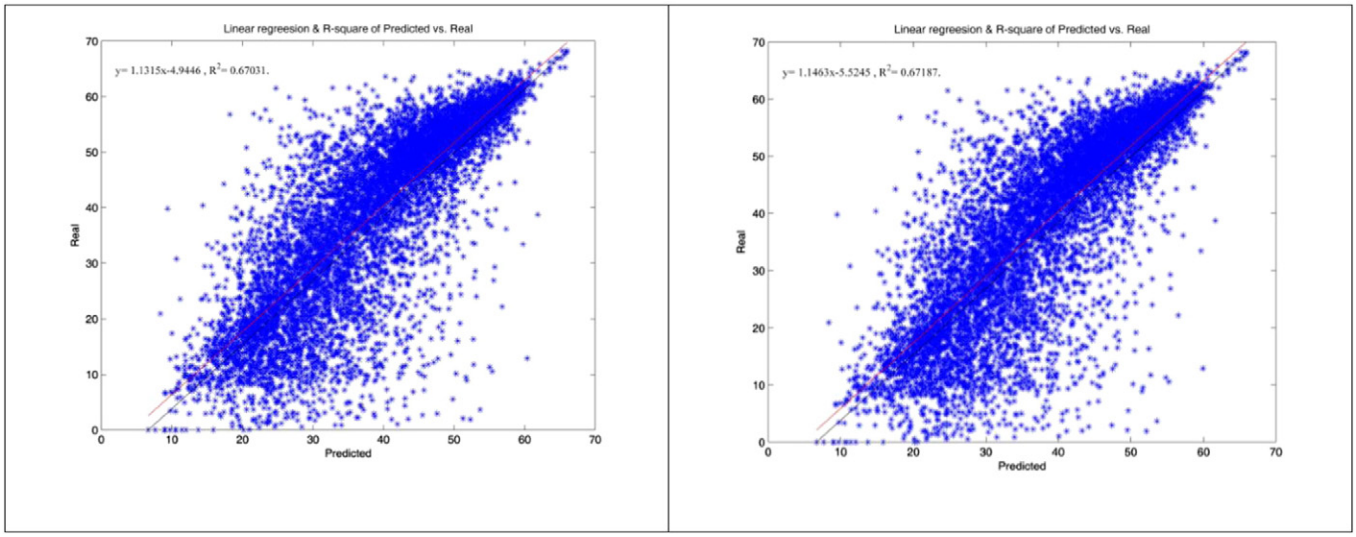

Fig. 7. Scatter plot between the real a predicted model (left: Ordinary and right: simple multi-Gaussian kriging) — black line: diagonal; red line: regression.

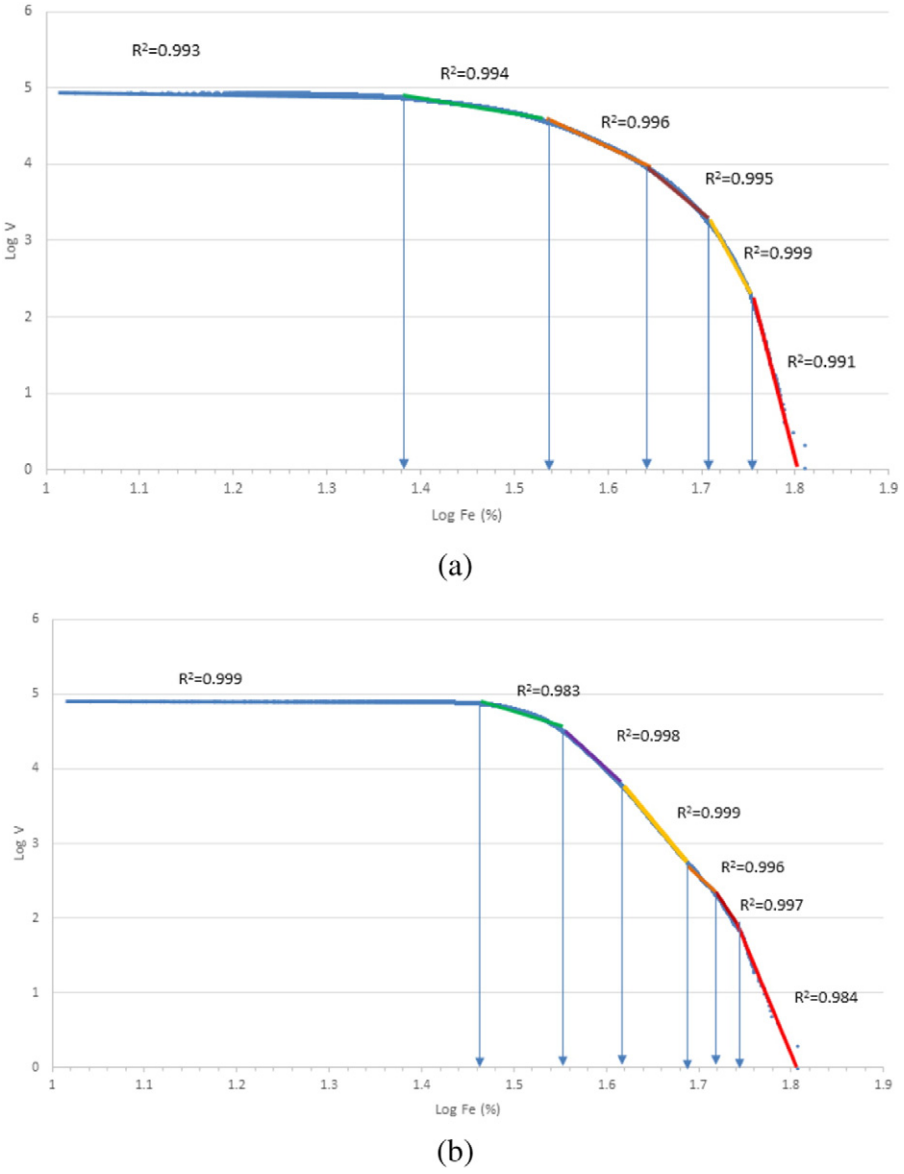

Fig. 8. C–V log–log plots obtained via the means of Mok (a) and Sok (b) estimation methods.

of nugget and spherical model (Sph) are fitted to the experimental semi-variogram. The estimated model of variogram is presented as follow:

$$\gamma(h) = 0.31 + 0.25Sph(20,\ 20,\ 11) + 0.16Sph(20,\ 20,\ 70) + 0.17Sph(20,\ 20,\ 180) + 0.04Sph(250,\ \infty,\ 250) + 0.07Sph(\infty,\ \infty,\ 250). \quad (3)$$

To implement the multi-Gaussian kriging in the case of both simple and ordinary, a block support of $10 \times 10 \times 12$ m^3 is defined with respect to geometrical shape of deposit and grid drilling dimensions (David, 1970) for the prediction of normalized Fe. Based on the 3D models, parts with Fe values higher than 50% occur in the NW and SE parts of the studied area which have been constructed by RockWorks software package (Fig. 6). The point support is deemed to preserve the primary variance of Fe. The search radii are set to 800, 800, and 400 in which two first ones are consistent with the horizontal and the last one with the vertical directions, respectively. Each block involves the prediction of mean grade above cut-off 0% to lunch the fractal analysis. This type of estimation provides the most compatible variability of Fe within the domains. Hence, these results are an input to the fractal analysis considering more populations.

Table 2
Mineralized zones' thresholds for Fe obtained by the C–V modeling based on the oMK and sMK estimation data.

Mineralized zone	Fe (%) thresholds based on oMK	Zone's range for Fe (%: oMK)	Fe (%) thresholds based on sMK	Zone's range for Fe (%: sMK)
Barren host rock	–	<24	–	<28
Very weak (A)	24	24–34	28	28–35
Weakly (B)	34	34–43	35	35–41
Moderately (C)	43	43–52	41	41–49
Highly (D)	52	52–56	49	49–52
Enriched (E)	56	>56	52	>52

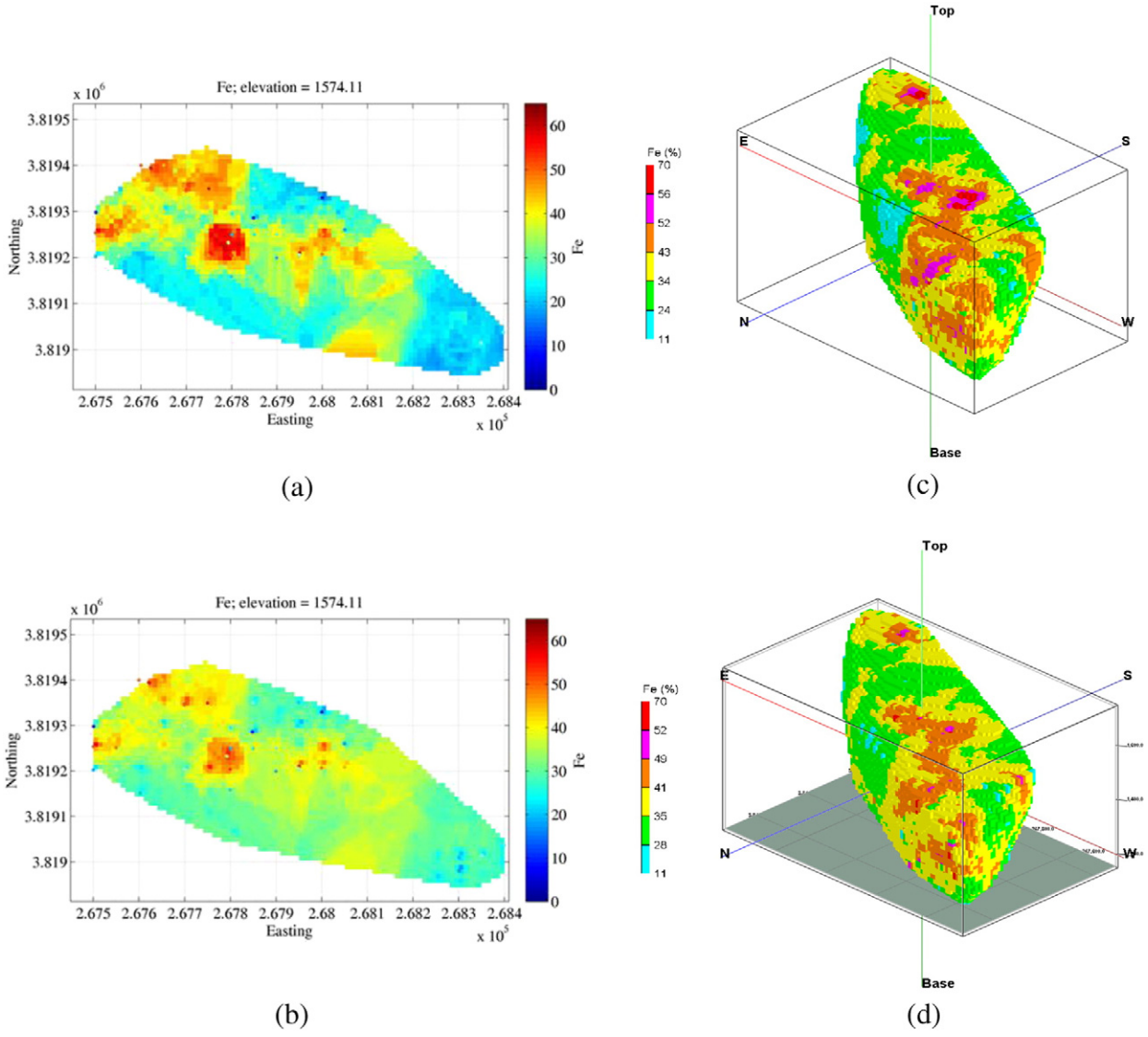

Fig. 9. Fe distribution at the level of 1574.11 m based on oMK (a) and sMK (b) and 3D model of C–V fractal modeling for oMK (c) and sMK (d).

All estimation methodologies require some technique to assess the underlying quality. Here, leave-one-out cross-validation is performed for the mean grade above 0% (Journel and Huijbregts, 1978). In this approach, each data is removed and re-estimated by the neighborhood data. Fig. 7 shows that both methods are performing satisfactory with respect to the statistics on the cross-validation errors as summarized in Table 1, while the scatter diagrams between true and estimated Fe grade are shown in Fig. 7. Small mean error and the slope regression tending to 1 suggest that both methods do not present bias estimation.

Table 3
Variances of Fe Mineralized zones obtained by the C–V modeling based on the oMK and sMK estimation data.

Mineralized zone	oMK variance	Zone's range for Fe (%: oMK)	sMK variance	Zone's range for Fe (%: sMK)
Barren host rock (A)	234.84	<24	248.90	<28
Very weak (A)	279.93	24–34	275.34	28–35
Weakly (B)	268.90	34–43	262.70	35–41
Moderately (C)	198.20	43–52	215.21	41–49
Highly (D)	118.40	52–56	121.70	49–52
Enriched (E)	58.85	>56	61.74	>52

6. Fractal modeling

Fe mineralized zones were separated based on the results obtained by the oMK and sMK using C–V fractal modeling. According to the C–V log–log plots, six and seven populations for Fe were distinguished based on the oMK and sMK estimation methods respectively, as depicted in Fig. 8. The fitted lines (segments) were obtained based on least-square regression method (Spalla et al., 2010). This regression was calculated with respect to R^2 values which vary between 0 and 1. If R^2 values are high and near to 1 so the segment has been better fitted (Davis, 2002). The barren host rocks have Fe values lower than 28% and 24% (based on oMK and sMK) obtained via the C–V log–log plots which occur in the marginal parts of the area (Table 2 and Fig. 9). Additionally, enriched zones derived via the sMK and oMK are higher than 52% and 56% which are present in small parts of the central, SE, W and NW parts of the area, as depicted in Table 2 and Fig. 9. According to the sMK and oMK interpolated results, the highly iron mineralized zones have Fe values 48–52% and 51–56% which occur in the central, SE, W and NW parts of the studied deposit (Fig. 9).

Consequently, the variances of different Fe populations derived via fractal modeling show that there is a similarity between trends of the variances' variations (Table 3 and Fig. 10). Variances derived

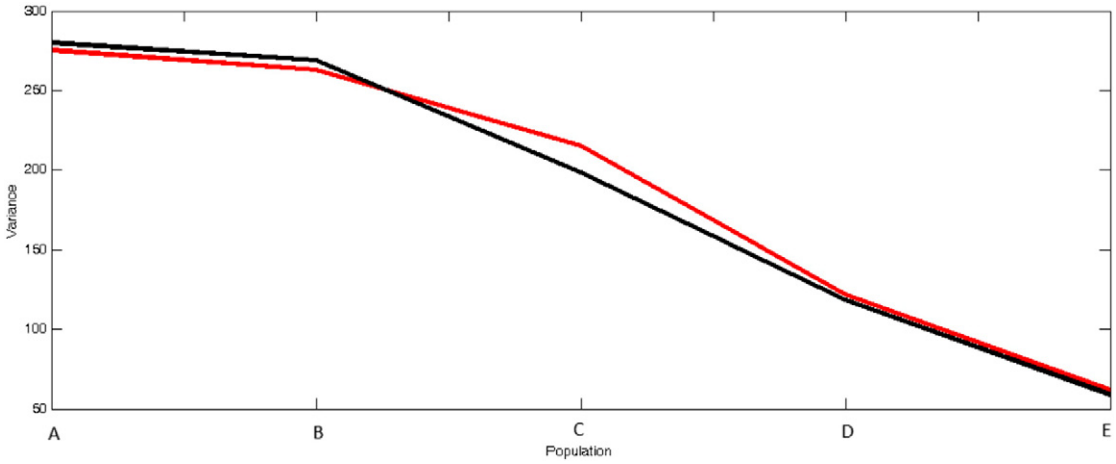

Fig. 10. Variances at the separated populations by the C–V fractal modeling (Red: sMK; Black: oMK).

via the oMK are lower than that for sMK in the moderately (41–49%), enriched (>56%) and highly (52–56%) Fe mineralized zones however; the values of variance within other mineralized zones are lower on the basis of sMK including barren host rocks (<24%), weakly (35–41%) and very weak (28–35%). As a result, this can be considered as criteria for optimization of mineralized zones' determination by the C–V fractal/multifractal modeling.

7. Post processing of the multi-Gaussian kriging

Prior to analysis on the local variability, it is of interest to review the produced estimated maps of oMK and sMK with their variances (Fig. 11). Separating the Fe populations by the C–V fractal modeling can characterize each domain entirely. The proper application of the multi-Gaussian kriging evaluates the tonnage, metal quantity and

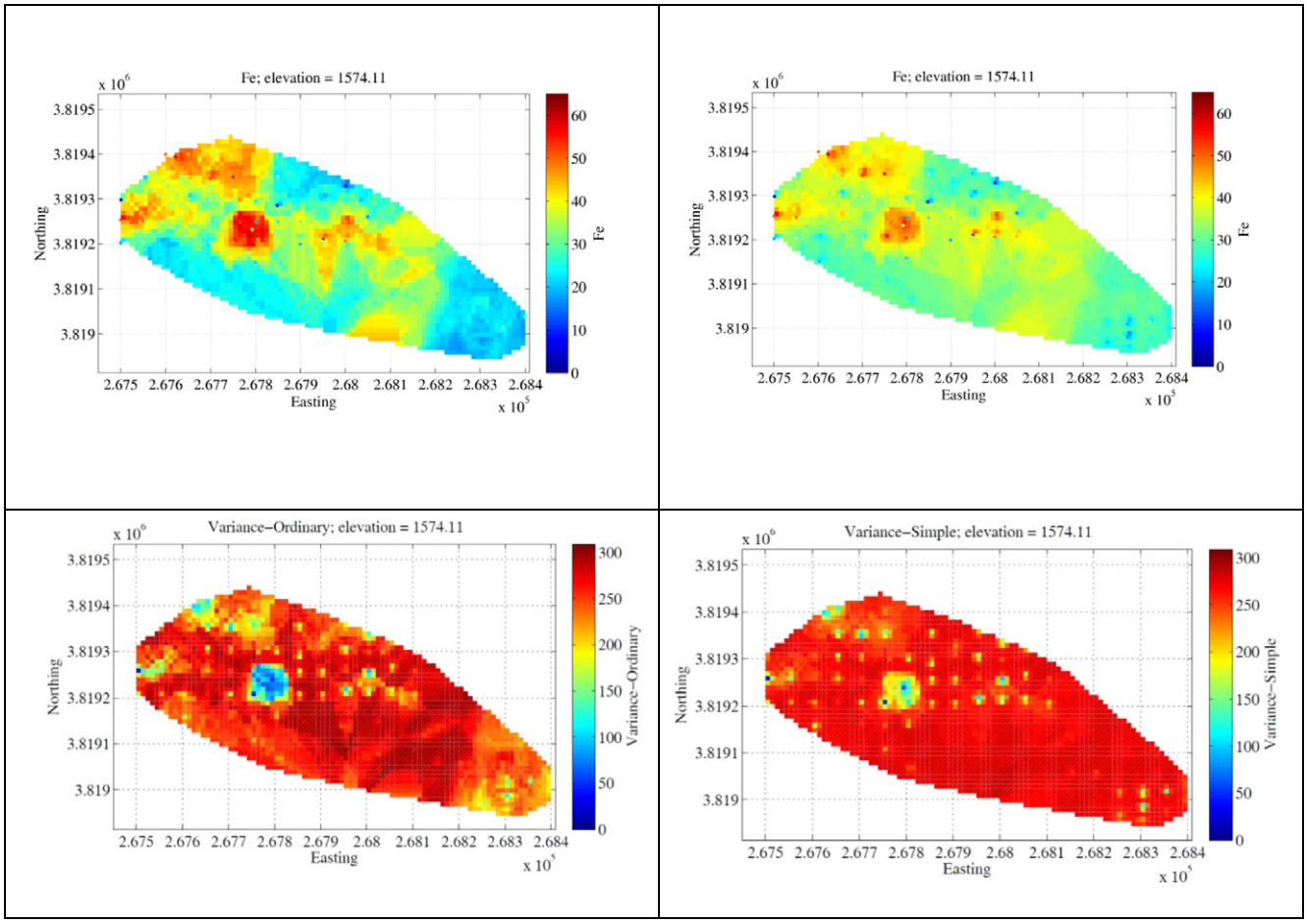

Fig. 11. Multi-Gaussian kriging; Top: estimation results; Bottom: local variance; Right: ordinary; Left: simple.

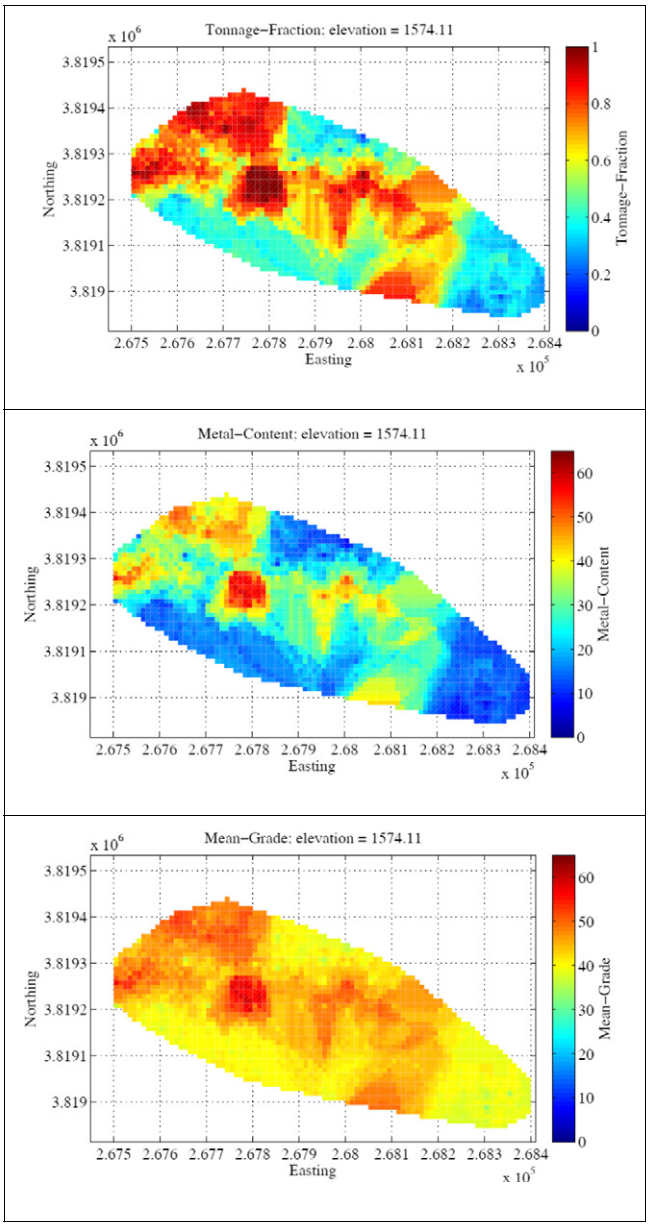

Fig. 12. Post processing of the ordinary multi-Gaussian kriging (oMk) for Fe values higher than the first threshold (24%).

mean grade above the specified threshold (e.g., >24% entitled "Commence of Fe mineralization": Fig. 12). These maps are one of the most effective mineral inventory information and are advantageous at different stages of ore body evaluations. They also provide an intuitive assessment of resources on the basis of exploratory data in the first step of the general size (tons of ore or quantity of metal) of the estimation within various cut offs. In this step, the estimates are neither resources nor reserves in the strict sense. During planning and production, these maps can be incorporated to the quantities of tones and metals to be mined over a specific time interval at the desired level by rapid insight in the changes of ore recoveries (Sinclair and Blackwell, 2006). As can be seen from Fig. 12, close to the central part of the deposit (elevation 1574.11 m, X = 267,800, Y = 3,819,200) somehow contain the significant tonnage, metal content and mean-grade above the desired cut offs, which show the commencement of the first population derived from the oMK.

8. Conclusion

Results obtained by the study show that multi-Gaussian kriging estimation methods are proper interpolation methods with several facilities such as assessing the tonnage, metal quantity and mean grade above the specified threshold, which are used for fractal/multifractal modeling. Comparison between results obtained by the C–V fractal modeling based on the oMK and sMK estimated data reveals that the variances of different mineralized zones are similar however; the appropriate variances belong to enriched and highly iron mineralized zones. Moreover, the moderately and weakly mineralized zones on the basis of sMK have variance values lower than that in oMK data.

Acknowledgment

The authors would like to thank Prof. Xavier Emery for his permission for using his programs and Mr. Ravanbakhsh Amiri as the executive manager of the Iran East Iron Ore Company (IEIOC) for authorizing the use of the Dardevey exploration dataset and Mrs Mania Qumarsy for her contribution to the reserve estimation. The authors also would like to acknowledge Mr. Farzan Rafia, Mr. Alireza Shivaei, Mr. Ali Hooman Arabshahi, Mr. Mohammad Seydi and Mrs. Mona Zandi, managers and personnel of Kavoshgaran Consulting Engineers Company for their valuable remarks.

References

Afzal, P., Fadakar Alghalandis, Y., Khakzad, A., Moarefvand, P., Rashidnejad Omran, N., 2011. Delineation of mineralization zones in porphyry Cu deposits by fractal concentration–volume modeling. J. Geochem. Explor. 108, 220–232.
Afzal, P., Fadakar Alghalandis, Y., Moarefvand, P., Rashidnejad Omran, N., Asadi Haroni, H., 2012. Application of power–spectrum–volume fractal method for detecting hypogene, supergene enrichment, leached and barren zones in Kahang Cu porphyry deposit, Central Iran. J. Geochem. Explor. 112, 131–138.
Afzal, P., Dadashzadeh Ahari, H., Rashidnejad Omran, N., Aliyari, F., 2013. Delineation of gold mineralized zones using concentration–volume fractal model in Qolqoleh gold deposit, NW Iran. Ore Geol. Rev. 55, 125–133.
Afzal, P., Alhoseini, S.H., Tokhmechi, B., Kaveh Ahangarana, D., Yasrebi, A.B., Madani, N., Wetherelt, A., 2014. Outlining of high quality coking coal by Concentration–Volume fractal Model and Turning Bands Simulation in East-Parvadeh Coal Deposit, Central Iran. Int. J. Coal Geol. 127, 88–99.
Agterberg, F.P., 2012. Multifractals and geostatistics. J. Geochem. Explor. 122, 113–122.
Agterberg, F.P., Cheng, Q., Wright, D.F., 1993. Fractal modeling of mineral deposits. In: Elbrond, J., Tang, X. (Eds.), 24th APCOM symposium proceeding, Montreal, Canada, pp. 43–53.
Armstrong, M., 1984. Problems with universal kriging. Math. Geol. 16 (1), 101–108.
Benndorf, J., Dimitrakopoulos, R., 2013. Stochastic long-term production scheduling of iron ore deposits: Integrating joint multi-element geological uncertainty. J. Min. Sci. 49 (1), 68–81.
Carranza, E.J.M., 2008. Geochemical Anomaly and Mineral Prospectivity Mapping in GIS. Handbook of Exploration and Environmental Geochemistry vol 11. Elsevier, Amsterdam, pp. 1–351.
Cheng, Q., 1999. Spatial and scaling modeling for geochemical anomaly separation. J. Geochem. Explor. 65, 175–194.
Cheng, Q., 2007. Mapping singularities with stream sediment geochemical data for prediction of undiscovered mineral deposits in Gejiu, Yunnan Province, China. Ore Geol. Rev. 32, 314–324.
Cheng, Q., Agterberg, F.P., 2009. Singularity analysis of ore-mineral and toxic trace elements in stream sediments. Comput. Geosci. 35 (2), 234–244.
Cheng, Q., Agterberg, F.P., Ballantyne, S.B., 1994. The separation of geochemical anomalies from background by fractal methods. J. Geochem. Explor. 51, 109–130.
Chilès, J.P., Delfiner, P., 2012. Geostatistics: Modeling Spatial Uncertainty. Wiley, New York.
Costa, J.F., 2003. Reducing the impact of outliers in ore reserves estimation. Math. Geol. 35 (3), 323–345.
Cressie, N., 1987. A nonparametric view of generalized covariances for kriging. Math. Geol. 19 (5), 563–586.
Cressie, N., Johannesson, G., 2001. Kriging for cut-offs and other difficult problems. geoENV III—Geostatistics for Environmental Applications. Springer, pp. 299–310.
Daneshvar, Saein L., Rasa, I., Rashidnejad Omran, N., Moarefvand, P., Afzal, P., 2012. Application of concentration-volume fractal method in induced polarization and resistivity data interpretation for Cu–Mo porphyry deposits exploration, case study: Nowchun Cu–Mo deposit, SE Iran. Nonlinear Process. Geophys. 19, 431–438.
David, M., 1970. Geostatistical Ore Reserve Estimation. Elsevier, Amsterdam (283 pp.).
Davis, J.C., 2002. Statistics and data analysis in Geology. John Wiley and Sons Inc, New York, pp. 1–638.

Delavar, S.T., Afzal, P., Borg, G., Rasa, I., Lotfi, M., Rashidnejad Omran, N., 2012. Delineation of mineralization zones using concentration–volume fractal method in Pb–Zn Carbonate hosted deposits. J. Geochem. Explor. 118, 98–110.
Deutsch, C.V., Journel, A.G., 1998. GSLIB: Geostatistical Software Library and User's Guide. second ed. Oxford University Press, New York, NY (369 pp.).
Deutsch, C.V., Rossi, M.E., 2014. Mineral Resource Estimation. Springer, New York.
Emery, X., 2006a. Multigaussian kriging for point-support estimation: incorporating constraints on the sum of the kriging weights. Stoch. Env. Res. Risk A. 20 (1–2), 53–65.
Emery, X., 2006b. Two ordinary kriging approaches to predicting block grade distributions. Math. Geol. 38 (7), 801–819.
Emery, X., 2006c. Ordinary multigaussian kriging for mapping conditional probabilities of soil properties. Geoderma 132 (1–2), 75–88.
Emery, X., 2007. Incorporating the uncertainty in geological boundaries into mineral resources evaluation. J. Geol. Soc. India 69 (1), 29–38.
Emery, X., 2008. Uncertainty modeling and spatial prediction by multi-Gaussian kriging: accounting for an unknown mean value. Comput. Geosci. 34 (11), 1431–1442.
Ghavi, J., Karimpour, M.H., 2010. Geological Investigation and Mineralization of the Dardway Iron deposit, Sangan Ore Field, Northeast Iran. The 1 st International Applied Geological Congress, Department of Geology, Islamic Azad University - Mashad Branch, Iran, pp. 26–28.
Golmohammadi, A., Karimpour, M.H., Malekzadeh Shafaroudi, A., Mazaheri, S.A., 2015. Alteration-mineralization, and radiometric ages of the source pluton at the Sangan iron skarn deposit. northeastern Iran Ore Geol. Rev 65, 545–563.
Goovaerts, P., 1997. Geostatistics for Natural Resources Evaluation. Oxford University Press, New York.
Guibal, D., Remacre, A.Z., 1984. Local estimation of the recoverable reserves: comparing various methods with the reality on a porphyry copper deposit. In: Verly, G., David, M., Journel, A.G., Mare'chal, A. (Eds.), Geostatistics for Natural Resources Characterization. Reidel, Dordrecht, pp. 435–448.
Hasanipack, A.A., Halaji, A., Rajaeian, F., 2009. Modeling and reserve evaluation of Dardevey deposit. Madankav Co (Persian Unpublished report).
Heidari, M., Ghaderi, M., Afzal, P., 2013. Delineating mineralized phases based on lithogeochemical data using multifractal model in Touzlar epithermal Au–Ag (Cu) deposit, NW Iran. Appl. Geochem. 31, 119–132.
Journel, A.G., 1980. The lognormal approach to predicting local distributions of selective mining unit grades. Math. Geol. 12 (4), 285–303.
Journel, A.G., Huijbregts, C.J., 1978. Mining Geostatistics. Academic Press, London.
Li, C.J., Zhao, N.L., Ma, T.H., 2002. Fractal reconstruction with unorganized geochemical data. Math. Geol. 34 (7), 809–829.
Li, C.J., Ma, T.H., Shi, J.F., 2003. Application of a fractal method relating concentrations and distances for separation of geochemical anomalies from background. J. Geochem. Explor. 77, 167–175.
Li, C.J., Ma, T.H., Chen, J.J., 2004. A fractal interpolatory approach to geochemical exploration data processing. Math. Geol. 36 (5), 593–606.
Lima, A., De Vivo, B., Cicchella, D., Cortini, M., Albanese, S., 2003. Multifractal IDW interpolation and fractal filtering method in environmental studies: an application on regional stream sediments of Campania region (Italy). Appl. Geochem. 18, 1853–1865.
Ma, T.H., Li, C.J., Lu, Z.M., 2014. Estimating the average concentration of minor and trace elements in surficial sediments using fractal methods. J. Geochem. Explor. 139, 207–216.
Malekzadeh Shafaroudi, A., Karimpour, M.H., Golmohammadi, A., 2013. Zircon U-Pb geochronology and petrology of intrusive rocks in the C-North and Baghak districts, Sangan iron mine. NE Iran J. Asian Earth Sci. 64, 256–271.
Mandelbrot, B.B., 1983. The Fractal Geometry of Nature. W.H. Freeman, San Fransisco (468 pp.).
Mao, S., Journel, A.G., 1999. Conditional 3D simulation of lithofacies with 2D seismic data. Comput. Geosci. 25 (7), 845–862.
Mare'chal, A., 1984. Recovery estimation: a review of models and methods. In: Verly, G., David, M., Journel, A.G., Mare' chal, A. (Eds.), Geostatistics for Natural Resources Characterization, Reidel, Dordrecht, pp. 385–420.
Matheron, G., 1971. The Theory of Regionalized Variables and its Applications. Ecole Nationale Supérieure des Mines de Paris, Fontainebleau (212 pp.).
Pyrcz, M.J., Deutsch, C.V., 2014. Geostatistical Reservoir Modeling. Oxford University Press.
Rahmati, A., Afzal, P., Abrishamifar, S.A., Sedeghi, B., 2015. Application of Concentration - Number and Concentration-Volume fractal models to delineate mineralized zones in the Sheytoor iron deposit, Central Iran. Arab. J. Geosci. 8, 2953–2965.
Reis, A., Sousa, A., Cardoso Fonseca, E., 2003. Application of geostatistical methods in gold geochemical anomalies identification (Montemor-O-Novo, Portugal). J. Geochem. Explor. 77 (1), 45–63.
Rivoirard, J., 1994. Introduction to Disjunctive Kriging and Nonlinear Geostatistics. Oxford University Press, Oxford, UK (181 pp.).
Sadeghi, B., Moarefvand, P., Afzal, P., Yasrebi, A.B., Daneshvar, Saein L., 2012. Application of fractal models to outline mineralized zones in the Zaghia iron ore deposit, Central Iran. J. Geochem. Explor. 122, 9–19.
Schofield, N., 1988. Ore reserve estimation at the Enterprise gold mine, Pine Creek, Northern Territory, Australia. Part 2: the multigaussian kriging model. CIM Bull. 81 (909), 62–66.
Shahbeik, S.h., Afzal, P., Moarefvand, P., Qumarsy, M., 2014. Comparison between Ordinary Kriging (OK) and Inverse Distance Weighted (IDW) based on estimation error Case study. Arab. J. Geosci 7. in Dardevey iron ore deposit, NE Iran, pp. 3693–3704.
Sinclair, A.J., Blackwell, C.H., 2006. Applied Mineral Inventory System. Cambridge University Press, London.
Soltani, F., Afzal, P., Asghari, O., 2014. Delineation of alteration zones based on sequential gaussian simulation and concentration–volume fractal modeling in the hypogene zone of Sungun copper deposit, NW Iran. J. Geochem. Explor. 140, 64–76.
Spalla, M.I., Morotta, A.M., Gosso, G., 2010. Advances in interpretation of geological processes: refinement of multi-scale data and integration in numerical modelling. Geological Society, London (240 pp.).
Stegman, C.L., 2001. How Doman Envelopes Impact on ihc Resource Estimate—Case Studies from the Cobar Gold Field, NSW, Australia, in Mineral Resource and Ore Reserve Estimation—the AusIMM Guide to Good Practice. In: Edwards, A.C. (Ed.), The Australasian Institute of Mining and Metallurgy: Melbourne. Mineral resource and ore reserve estimation: the AusIMM guide to good practice 23, pp. 221–236 (p. 221).
Subbey, S., Christie, M., Sambridge, M., 2004. Prediction under uncertainty in reservoir modeling. J. Pet. Sci. Eng. 44 (1), 143–153.
Verly, G., 1983. The multigaussian approach and its applications to the estimation of local reserves. Math. Geol. 15 (2), 259–286.
Verly, G., 1984. The block distribution given a point multivariate normal distribution. Geostatistics for natural resources characterization. Springer, pp. 495–515.
Wang, G., Pang, Z., Boisvert, J.B., Hao, Y., Cao, Y., Qu, J., 2013. Quantitative assessment of mineral resources by combining geostatistics and fractal methods in the Tongshan porphyry Cu deposit (China). J. Geochem. Explor. 134, 85–98.
Yasrebi, A.B., Afzal, P., Wetherelt, A., Foster, P., Esfahanipour, R., 2013. Correlation between geological and concentration–volume fractal models for Cu and Mo mineralised zones separation in Kahang Porphyry Deposit, Central Iran. Geol. Carpath. 64 (2), 153–163.
Yasrebi, A.B., Wetherelt, A., Foster, P., Coggan, J., Afzal, P., Agterberg, F.P., Kaveh Ahangaran, D., 2014. Application of a density–volume (D–V) fractal model for rock characterisation and correlation of RQD and lithological units with density model in the Kahang porphyry deposit, Central Iran. Int. J. Rock Mech. Min. Sci. 66, 188–193.
Zuo, R., Wang, J., 2015. Fractal/multifractal modeling of geochemical data: a review. J. Geochem. Explor. http://dx.doi.org/10.1016/j.gexplo.2015.04.010.
Zuo, R., Cheng, Q., Agterberg, F.P., Xia, Q., 2009. Application of singularity mapping technique to identify local anomalies using stream sediment geochemical data, a case study from Gangdese, Tibet, western China. J. Geochem. Explor. 101, 225–235.
Zuo, R., Carranza, E.J.M., Cheng, Q., 2012. Fractal/multifractal modelling of geochemical exploration data. J. Geochem. Explor. 122, 1–3.
Zuo, R., Xia, Q., Wang, H., 2013. Compositional data analysis in the study of integrated geochemical anomalies associated with mineralization. Appl. Geochem. 28, 202–221.